

Recognition of Minerals Using Multispectral Remote Sensing Data: A Case Study in the Sultanate of Oman

Sankaran Rajendran^{1*} and Sobhi Nasir²

¹Department of Earth Sciences, College of Science, Sultan Qaboos University, P.O. Box: 36, Al-Khod, PC 123, Muscat, Sultanate of Oman, ²Center for Earth Sciences, Sultan Qaboos University, P.O. Box: 36, Al-Khod, PC 123, Muscat, Sultanate of Oman. *Email: rajendra@squ.edu.om.

ABSTRACT: The present study demonstrates the capability of a multispectral sensor for the detection of the minerals in the rocks surrounding the Rusayl and Al Jafnayn regions, Sultanate of Oman. The study of spectral absorptions of rocks and minerals in the visible and near infrared (VNIR) and short wavelength infrared (SWIR) spectral bands of the Advanced Spaceborne Thermal Emission and Reflection Radiometer (ASTER) using the Spectral Angle Mapper (SAM) supervised image classification technique has provided information on the occurrence of minerals in the rock types of the regions. The study shows the occurrence of carbonate minerals in the limestone formations and of poorly altered silicate minerals in the basic dyke rocks of the study regions. The analysis of minerals over the ancient terraces and recent alluvial deposits show that the deposit materials are derived from the dykes and foliated gabbro source rocks. The image interpretation is compared to the geological map, verified in the field and confirmed through laboratory analyses. The satellite data and the image processing techniques used have potential in the recognition of minerals in the rocks of the study region and could be used in similar arid regions elsewhere in the world.

Keywords: Minerals mapping; Spectral absorptions; SAM; ASTER; Sultanate of Oman.

التعرف على المعادن باستخدام بيانات الاستشعار عن بعد المتعدد الأطياف: حالة دراسية من سلطنة عمان

سَنكران راجيندران و صبحي نصر

ملخص: تبين هذه الدراسة قدرة الاستشعار متعدد الأطياف على التعرف على معادن الصخور في مناطق الرسيل والجفنين بسلطنة عمان. تسهم دراسة الامتصاص الطيفي للمعادن والصخور في تقديم معلومات حول مناطق تواجد المعادن والصخور ضمن النطاقات الطيفية المرئية للأشعة تحت الحمراء وتحت الحمراء قصيرة الموجة للانبعاش الحراري الفضائي والإشعاع المنعكس، وباستخدام زاوية المخطط الطيفي لطريقة تصنيف معالجة الصور. تبين الدراسة الحالية تواجد المعادن الكربوناتيية ضمن وحدات صخور الحجر الجيري، وتواجد معادن السيليكات، المتغيرة قليلاً بالتجوية، ضمن قواطع الصخور النارية القاعدية، في مناطق الدراسة. كما بينت دراسة المعادن المكونة للمدرجات الصخرية القديمة وفي الرواسب الغرينية الحديثة على أن مصدر هذه الرواسب قادم من القواطع ومن الجابرو الطيفي. تم دراسة التفسيرات والنتائج عن طريق الخرائط الجيولوجية والتحقق الميداني والتأكد عن طريق التحاليل المخبرية. تثبتت بيانات وطرق معالجة صور الأقمار الصناعية إمكانيتها في التعرف على المعادن المكونة للصخور في منطقة الدراسة، والتي يمكن استخدامها في المنطقة القاحلة المشابهة في أماكن أخرى من العالم.

مفتاح الكلمات: المسح المعدني، الامتصاص الطيفي، الماسح الطيفي الزاوي (سام)، أُنطقة الاستشعار الحراري المتقدم (أستر)، سلطنة عمان.

1. Introduction

Remote sensing is a cost-effective alternative technique to other expensive and time-consuming tools for mapping different lithological units and structures in geological studies. The technique is widely used in regions which have extremely rugged topography where it is difficult to do dense sampling and detailed conventional geological mapping. Multispectral satellite images acquired by remote sensing play a vital role in mapping of lithological

formations and have the capability of providing information on the occurrence and distribution of minerals and rocks [1-8]. Satellite data and image processing techniques are used to map ophiolite sequences, chromite potential zones, hydrothermal mineralized zones, carbonates and carbonatite rocks in the arid region of the Sultanate of Oman [1, 9-12]. Studies using hyperspectral remote sensing data have also been carried out on the Oman ophiolite sequences [13-18]. However, study of the application of multispectral remote sensing technique to the occurrence of minerals within rocks is limited. It is potentially important in the field of geological mapping and exploration of mineral resources and useful for exploration and mining companies. Therefore, in the present study, an attempt is made to demonstrate the capability of multispectral ASTER satellite data in the recognition of minerals and rock types of the Rusayl and Al Jafnayn regions, near Muscat in the Sultanate of Oman (Figure 1) using VNIR and SWIR spectral bands by applying the Spectral Angle Mapper (SAM) supervised image classification method. The spectral sensitivity of carbonate rocks of the regions in ASTER VNIR-SWIR-TIR spectral bands has been studied by Rajendran and Nasir [19].

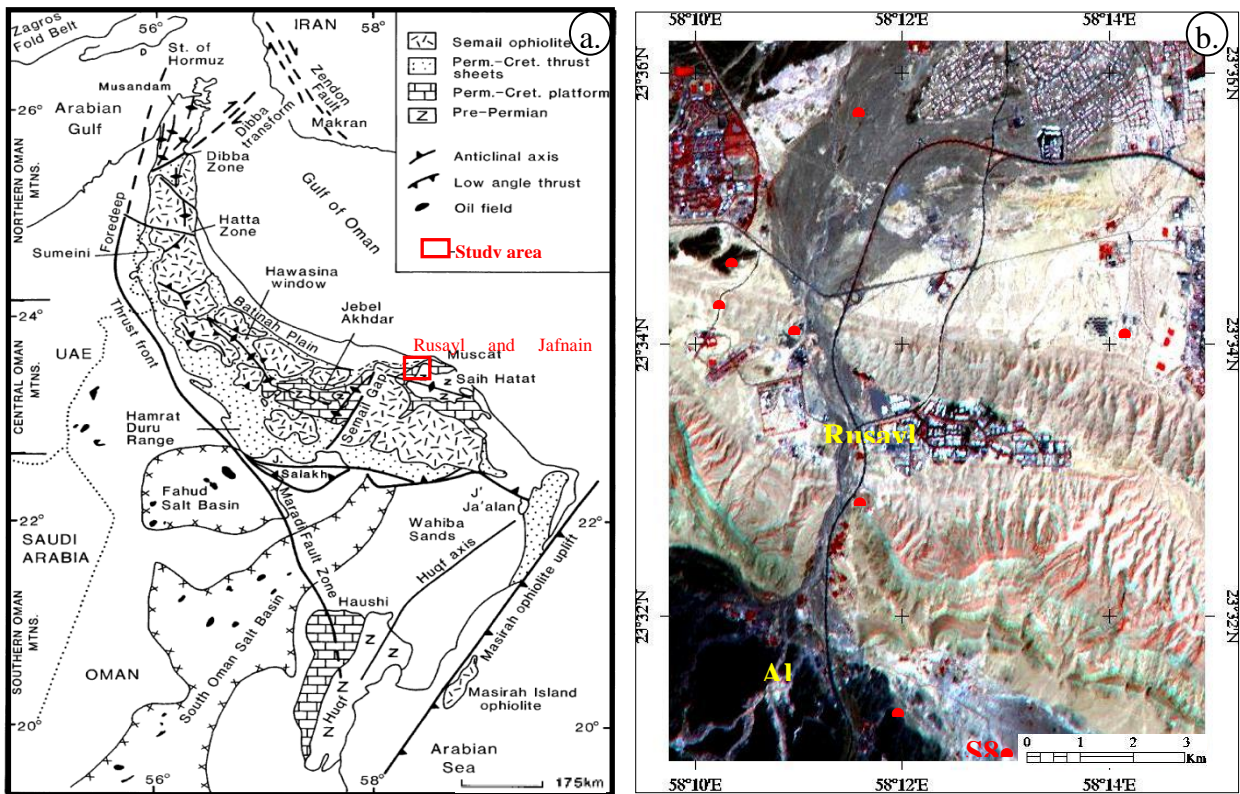


Figure 1. (a) Regional geology and structure map of the Oman Mountain area (after [20]) showing the location of the Rusayl and Al Jafnayn region, (b) the ASTER RGB image (R:3; G:2; B:1) showing the sample locations in the study region.

2. Geology of the Rusayl and Al Jafnayn regions

The geology in and around the Rusayl and Al Jafnayn region was studied by Rajendran and Nasir [19]. The region mainly consists of sedimentary formations of Tertiary and Quaternary age which are underlain by an allochthonous unit, the Semail nappe (Figure 2). The major rock types of the region are lower nodular limestones (Lm) and upper nodular limestones (Ulm) of Tertiary age distributed at the centre of the region. The alluvial fans and wadi alluvium of Recent to Sub-Recent Quaternary age occur between the lower and upper nodular limestones. The lower nodular limestone is associated with fossilized yellow marl formations (Ym- interlayered by brown sandstone, and Yml- Yellow marl with large foraminifera), whereas the upper nodular limestone is mainly associated with the Recent to Sub-Recent alluvial fan sediments (Rlm). The alluvial terrace consists of materials from dykes and gabbros dominated by the iron-rich mafic silicate minerals. The occurrence and spatial distribution of other sedimentary formations of the region are shown in Figure 2. Sheeted dyke (SD), consisting of doleritic and basaltic dykes occurs in the SW of the region.

MINERALS MAPPING USING REMOTE SENSING DATA

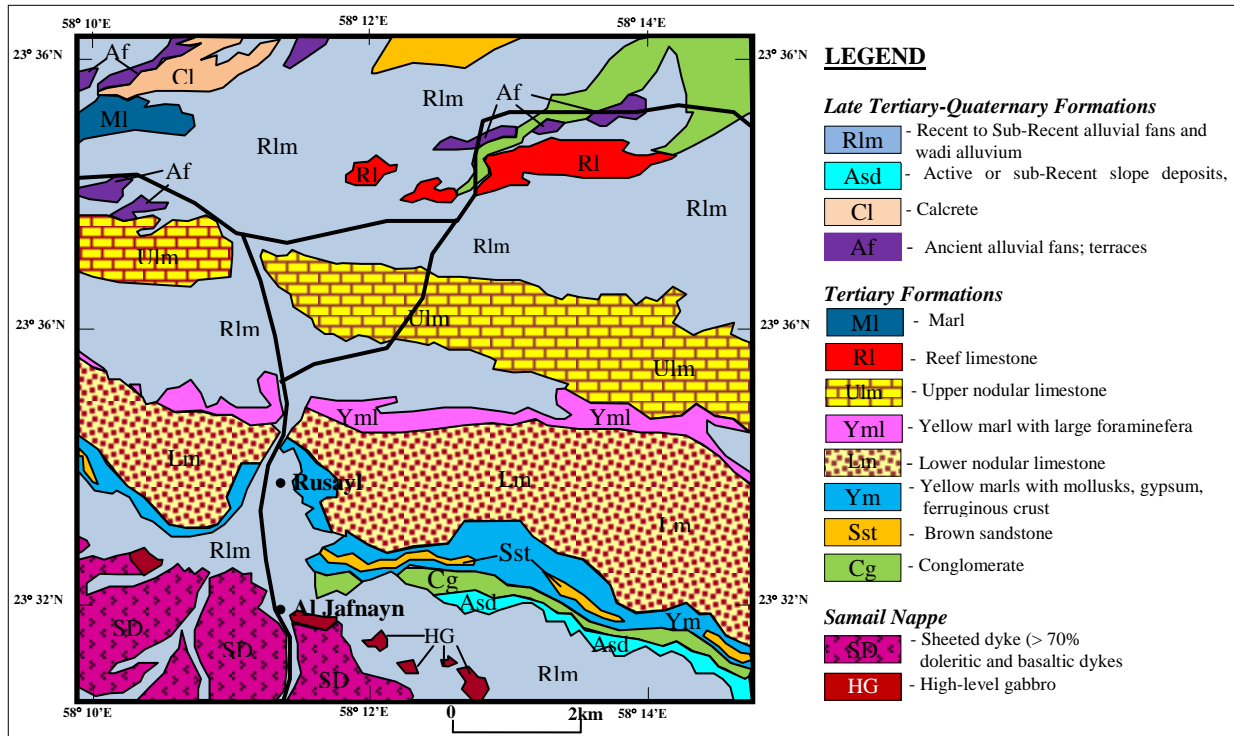


Figure 2. Geological map of the Rusayl and Al Jafnayn region [19, 21].

3. Spectral characteristics of minerals and rocks

Minerals in rocks respond uniquely to different electromagnetic wavelengths and create a diagnostic spectral signature [22, 23] which conveys information on the composition of the rocks. Several studies on minerals and rocks using absorption features of reflectance spectra in the spectral bands have been conducted by a number of authors [23-32]. Hunt and Salisbury [33], Hunt *et al.* [34], Hunt and Ashley [35] and Blom *et al.* [36] have studied the spectra of fresh and weathered surfaces of igneous rocks and stated that strong absorptions in the spectrum of visible and near infrared region are due to the presence of iron contents. The ferrous iron (Fe^{+2}) in the octahedral coordination of clinopyroxene (high Ca-pyroxene) causes an absorption of around 1.0-1.1 μm and in the six fold coordination of olivine and pyroxenes, produces around 0.9-1.1 μm due to the electronic transition. Olivine produces broad absorption around 1 μm . The ferric iron (Fe^{+3}) in weathering products is responsible for absorption at wavelengths shorter than about 0.55 μm due to the charge transfer, giving rise to the visible red color which is characteristic of 'iron staining'. The vibrations involving the OH stretch and metal-OH bend occur within the 2.0 to 2.5 μm wavelength region. The Al-OH and Mg-OH minerals show absorptions close to 2.2 μm and 2.3 μm respectively [31, 37]. In addition to this, the carbonate minerals such as calcite ($CaCO_3$) and dolomite ($CaMg(CO_3)_2$) have diagnostic spectral absorption features which can be used to distinguish them from each other [24, 26-29, 38]. Hunt and Salisbury [33] found that the calcite absorption is centered at 2.35 μm and dolomite at 2.33 μm . In 1994, Van der Meer concluded that calcite absorption is centered at 2.3465 μm and dolomite at 2.3039 μm . Recent studies carried out by Rajendran *et al.* [12], Rajendran and Nasir [19, 39], Mars and Rowan [40], Combe *et al.* [15] and Clenet *et al.* [18] have described the absorption characters of the carbonate and silicate minerals of certain rocks in Oman. Study of Rajendran *et al.* [12] shows that the major rocks of the study region are the carbonate rocks (lower nodular limestones and upper nodular limestones) and the sheeted basaltic dykes. There are also minor occurrences of the Recent to Sub-Recent alluvial fans and wadi alluvium. The limestone predominantly consists of dolomite and calcite carbonate minerals, and the dykes are rich in pyroxenes, amphiboles and plagioclase silicate minerals. The minerals of the rock types are recognisable from satellite images that cover the wavelengths discussed above.

To understand in detail the absorption characters of such minerals and rocks in the VNIR and SWIR regions, the spectral plots of the major minerals (Fig. 3a, spectra offset for clarity stacked from the USGS Spectral Library for minerals, Envi 5) and rocks (Figure 3b, spectra stacked from the Johns Hopkins University Spectral Library, Envi 5) are given in Figure 3. The carbonate minerals (calcite and dolomite) show absorptions of around 2.3 μm (line of carbonate absorptions) due to C-O bonding in their contents, and the silicate minerals such as olivine, augite, enstatite, hypersthene and hornblende show absorptions in the range of 0.9-1.1 μm (the region of iron absorptions) due to the presence of ferrous iron in their coordination. Minerals like hornblende and mica show light and shallow absorptions in 1.4 μm and 2.3 μm due to the presence of the OH groups in their contents. The plagioclase and quartz show absorptions around 0.6 μm , 1.4 μm and 2.1 μm . The absorptions of such mineral bearing rocks as limestone (fossiliferous limestone) and dykes (basalt and diabase) show strong major absorptions around 2.3 μm and 1.1 μm respectively. The absorption of limestone around 2.3 μm is due to the presence of carbonate minerals in the rock and

absorptions around 1.1 μm are due to the presence of the iron-rich major silicate minerals in the dyke rocks. Since the ASTER spectral band 8 falls in SWIR region is characteristic to diagnostic CO₃ absorption near 2.31–2.33 μm wavelengths, the band can be used to detect the carbonate minerals and discriminate rocks bearing them. As well as this, the ASTER band 3 can be used to detect the iron-rich minerals (which have absorptions around 0.9–1.1 μm wavelengths) and discriminate mineral bearing rocks like dykes. Also, the hydroxyl and water molecule bearing rocks have absorptions around 1.4 μm , 1.9 μm and 2.3 μm , and these can probably be detected in the ASTER bands 4 and band 8. The ASTER band 6 facilitates the mapping of mica and clay minerals due to Al–OH absorption occurring close to a 2.20 μm wavelength [40–42].

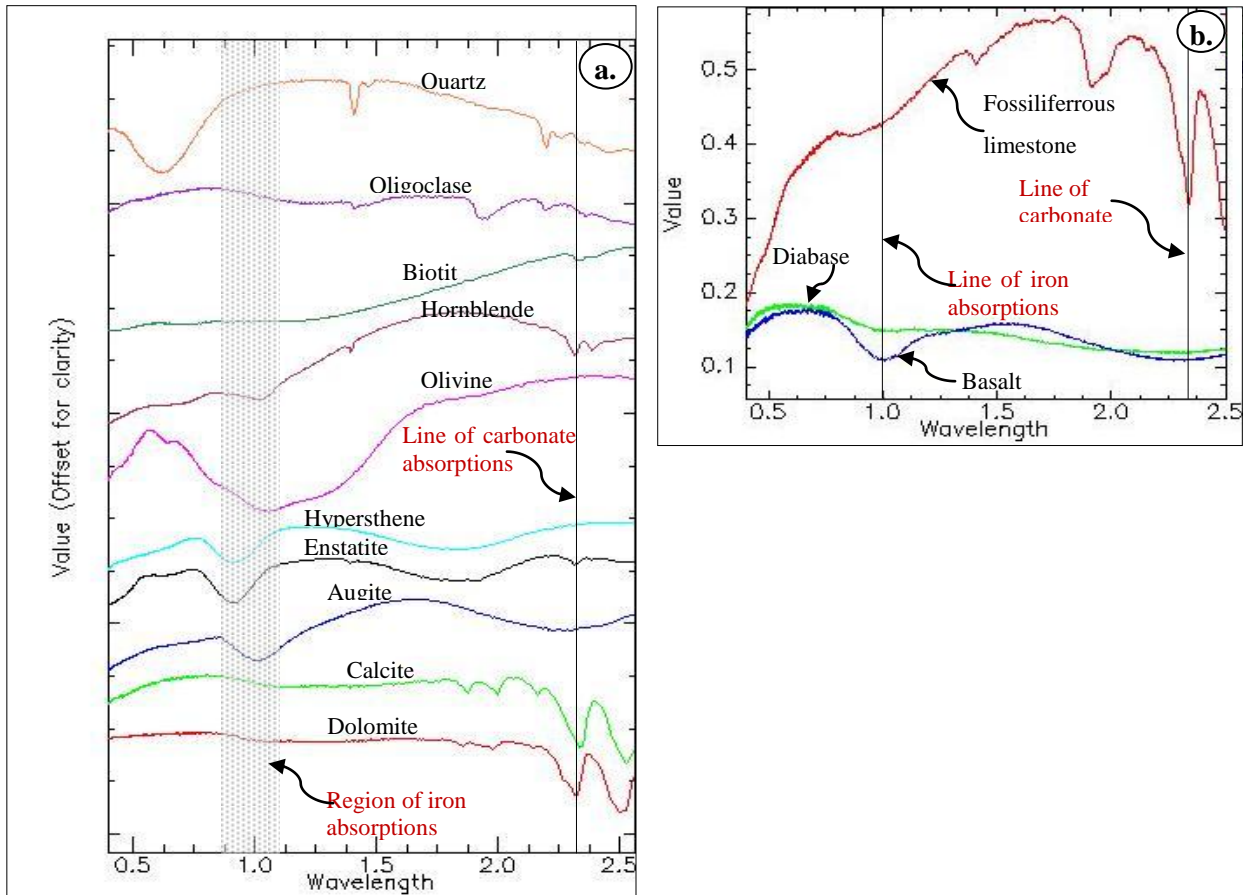


Figure 3. Spectral plots of (a) the major minerals (spectra offset for clarity) and (b) the rocks of the study region showing the carbonate and iron absorptions in the VNIR-SWIR regions.

4. Satellite data

ASTER data have frequently been used to map silicate and carbonate rocks of arid regions, as well as for volcanic studies [39, 40, 43–46]. There is an ASTER sensor on board the earth-observing system (EOS) TERRA platform, launched in December 1999 [47]. This sensor records visible reflected radiation in three spectral bands (VNIR between 0.52 and 0.86 μm , with 15-m spatial resolution), shortwave infrared reflected radiation in six spectral bands (SWIR between 1.6 and 2.43 μm , with 30-m spatial resolution) and emitted thermal infrared radiation in five spectral bands (between 8.125 and 11.65 μm , with 90-m spatial resolution) (Table 1). It also records the data in band 3B (0.76–0.86 μm) with a backward looking angle that enables the calculation of Digital Elevation Model (DEM). The inclusion of spectral bands in the SWIR region enhances the surface mineralogical and lithological mapping.

In the present study, 14 ASTER Level 1B (L-1B) data (AST_L1B_00303292004065157_20101106004827_15688) dated March 29, 2004 of the study region were obtained from NASA Land Processes Distributed Active Archive Center User Services, USGS Earth Resources Observation and Science (EROS) Center (<https://lpdaac.usgs.gov>). The data were received in Tag Image File (TIF) Format which provides files for each band containing the imagery and an ASCII text. meta file containing the metadata. These were supplied in terms of scaled radiance at-sensor data with radiometric and geometric corrections applied. The images were checked and found to be cloud cover of 0% and were rectified for sensor errors, such as banding and other geometric distortions. The images were georeferenced in the UTM projection and WGS-84 ellipsoid datum. We used nine VNIR and SWIR spectral bands of the study area resampled to 15 mts. spatial resolution. The data were processed and interpreted to demonstrate the occurrence of minerals in the rocks using ENVI (5) and ArcGIS (10.1) software.

MINERSLS MAPPING USING REMOTE SENSING DATA

Table 1. Sensor characteristics of ASTER instruments.

Sensors	<u>ASTER</u>		
	VNIR	SWIR	TIR
Spectral bands with range (µm)	Band 01 0.52–0.60 Nadir looking	Band 04 1.6–1.7	Band 10 8.125–8.475
	Band 02 0.63–0.69 Nadir looking	Band 05 2.145–2.185	Band 11 8.475–8.825
	Band 03N 0.76–0.86 Nadir looking	Band 06 2.185–2.225	Band 12 8.925–9.275
	Band 03B 0.76–0.86 Backward looking	Band 07 2.235–2.285	Band 13 10.25–10.95
		Band 08 2.295–2.365	Band 14 10.95–11.65
		Band 09 2.36–2.43	
Spatial Resolution (m)	15	30	90
Swath width (km)	60	60	60
Radiometric Resolution (bits)	8	8	12
Cross Track Pointing	± 318km (± 24 deg)	± 116km (± 8.55 deg)	± 116km (± 8.55 deg)

5. Methodology

Initially, the major rock types of the Rusayl and Al Jafnayn region were discriminated by developing a simple colour composite image [19, 48] using the ASTER spectral bands 8 (2.295–2.365 µm), 3 (0.78–0.86 µm), and 1 (0.52–0.60 µm). Here, the band 8 was chosen to show the carbonate minerals bearing limestone formations, and the ASTER bands 1 and 3 are selected to characterize the iron bearing silicate minerals and dyke rocks of the region. Subsequently, the minerals of the rock types of the region were studied using SAM method based on the “Spectral Hourglass” scheme [12, 49-51]. SAM encompasses tools such as Minimum Noise Fraction (MNF) transformation, Pixel Purity Index (PPI) and n-Dimensional visualizer, and classifies minerals based on library spectra [12, 49-52]. The SAM method is one of the widely accepted and popular image processing techniques for hyperspectral image processing, which can also be used in lower spectral resolution systems [12, 49-53]. The method applied on VNIR and SWIR spectral bands determined the inherent dimensionality of MNF image data [54] which contains the increase of noise from MNF bands 1 to 9. These bands were further processed to determine the most spectrally pure pixels, and contain mineral information of the image by PPI providing the PPI iteration value of 10,000 (the maximum), the default threshold value of 2.5 and the SAM angle of 0.15 in radians. The default angle value of 0.10 set at the SAM procedure provided 8046 unclassified image pixels (which is about 2.5% of the total number of pixels of 3,21,114). By increasing the SAM angle to 0.15, the pixels were fully classified mainly within the n-D class #1 and n-D class #7. The obtained pure pixels typically correspond to the mixing endmembers computed by repeatedly projecting n-D scatter plots on a random unit vector. Figure 5 shows the group of pure pixels in the n-Dimensional visualizer plot (Figure 5a) and the number of pure pixels extracted as endmembers with chosen colors (Figure 5b). Figure 6 shows the spectra (n-D class Mean) derived, based on endmembers with respect to the colors. Figure 7 is the SAM classified image showing the occurrence of minerals of the region. Table 2 provides details of the number of pixels, classified by their relative percentages and the total areas of their distribution. To study and understand the occurrence and spatial distribution of predominant minerals of the rocks of the region, the images of n-D classes 3, 6, 7 and 9 are given in Figure 8. The regional geological map [21] was used to verify the processed images and confirm the occurrence of minerals and rocks in the study region.

Finally, the interpreted images were evaluated in field and laboratory studies. During the field work, traverse based sample collection of minerals and rocks were carried out. The samples were used for spectral measurements, megascopic, microscopic, and mineral studies at the laboratory of the Department of Earth Sciences and Central Analytical and Applied Research Unit (CAARU), Sultan Qaboos University, to validate the occurrence of minerals in the rocks and confirm the interpretation of images. The petrological characters of rocks and minerals of the study region were studied under microscope by preparation of thin sections of samples. To confirm the capability of sensor and characters of the spectral bands used in this study, the reflectance spectra of samples were measured using a PIMA SP infrared spectrometer and studied. This instrument was fabricated for field spectroscopy by Integrated Spectronics Pty Ltd., Australia to verify processed remote sensing data. The instrument identified and analyzed the spectral signal

of minerals in the wavelength ranges from 1300 to 2500 nm with PIMA VIEW software (version 3.1). The spectral resolution of the device was ~ 7 nm. It has a built-in wavelength calibration target plate and is capable of measuring spectra from 10 seconds to around 5 minutes speed. Moreover, the samples used for spectral studies and other selected samples were further analysed for identification of minerals to confirm the image interpretations, field and microscopic studies by X-ray powder diffraction, using X'Pert PRO (P Analytical Company, The Netherlands) at CAARU, working based on PW1710 (Cu: 1.54).

6. Mapping of rock types and recognition of minerals

The discrimination of similar rock types occurring in parts of Sultanate of Oman using ASTER spectral bands is described by Rajendran *et al.* [10-12, 48] and Rajendran and Nasir [9, 19, 39, 51]. In this study, the colour composite image developed [12, 39] and studied using the ASTER spectral bands 8 (2.295–2.365 μm), 3 (0.78–0.86 μm), and 1 (0.52–0.60 μm) of the study region is given in Figure 4. The image shows those formations rich in carbonate minerals in shades of bright colors, discriminating them from the dark coloured sheeted dykes and ancient alluvial terrace deposits. The alluvial fan materials which are derived from the dykes and gabbros appear in light brown, which distinguishes them from wadi alluviums showing in shades of bright colours. However, the wadi alluviums are not discriminated well from the adjacent source rocks rich in carbonate minerals. The alluvial fan deposits consisting of the materials of dykes and gabbros derived from the mafic rock source region are clearly discriminated on the image. As interpreted, the rocks and formations correlate with the geological map (Figure 2).

The SAM image (Figure 7) shows the occurrence and spatial distribution of different minerals that occur in various proportions in different rock types of the region. The occurrence and spatial distribution of minerals within different lithologies of the region can be identified from the selected colors of end member spectra (Figures 5a, b and 6) and interpreted with the geology of the region (Figure 2) [12, 51].

The SAM classified image (Figure 7) showed the area of 1.8117 km^2 by red pixels based on n-D class #1. The end member mean spectra of n-D class #1 (Figure 6) show the absorptions in bands 4 (1.6–1.7 μm) and band 7 (2.235–2.285 μm). The clustered pixels along the wadi flow and built-up land regions (Figure 7) represent the presence of vegetation. The strong absorptions in bands 4 and 7 (OH and CO_3 stretched) are due to the chlorophyll content in the vegetation occurring in these areas. The occurrence of vegetation was confirmed by the ASTER RGB (1-3) image of the area (Figure 1b) and validated during the field check. The occurrence and spatial distribution of carbonate minerals (calcites) over about 0.0447 km^2 is shown in green, detected by n-D class #2, and about 30.3601 km^2 of dolomites are represented in blue by the n-D class #3 [12, 51]. The spectra of both classes show carbonate absorptions (decrease in trend) in band 8, whereas the absorption in band 5 may be due to the presence of Ca and Mg contents in the minerals. The absorption in band 3 of the spectra may be due to the iron content present in the clay minerals (in marl) that are associated with the dolomites, as discussed in section 7. The pixels representing the dolomite minerals are found in areas where limestone formations occur (Figure 7).

Figure 8a shows the occurrence and spatial distribution of dolomite minerals in the lower nodular limestone and upper nodular limestone regions (Figure 2). Such mineral-bearing carbonate formations were verified during the field work [19] and studied in the laboratory as discussed in section 7. The minor occurrence and spatial distribution of water and hydroxyl group bearing clay minerals in the marls which is associated in limestones were detected in the n-D class #4 (about 2.0808 km^2 , in yellow) and n-D class #5 (about 0.3924 km^2 in cyan). The spectra belonging to these minerals show absorptions in spectral bands 3, 5 and 7 due to the presence of iron, magnesium and calcium, and to the hydroxyl group present in the minerals respectively. The minerals are found in the limestone formations that appear in blue in the figure. The occurrence of such minerals was verified in the field where small streams originate, these flowing both parallel and perpendicular to the limestone formations, and where the marls occur.

The n-D class #6 (12.2553 km^2) and n-D class #7 (17.2129 km^2) are represented in magenta and maroon respectively. These are more significantly distributed in the places where dyke and gabbro rocks and derived materials are found in the wadi alluvium. The presence of such pixels are due to the occurrence of silicate minerals such as clinopyroxene, orthopyroxene, amphibole, and plagioclase minerals, the basic constituents occurring in variable proportions in the poorly altered rocks [12, 51]. Both the endmember spectra show poor absorptions in bands 3, 4 and 7 due to iron, magnesium and calcium, and aluminium contents in the minerals of the rock. The occurrence of pink pixels separately from the maroon pixels, in the region of occurrence of dyke and gabbro rocks, represents the presence of unaltered silicate minerals in the rocks. On the other hand, maroons mixed with pink colored pixels occur in areas of wadi alluvium and clay minerals, and represent the presence of poorly altered silicates and aluminium silicate minerals. Figures 8b and c show the occurrence and spatial distribution of silicate minerals. The n-D class #8 (0.229 km^2 , sea green colored pixels) shows poor occurrences of silicate minerals and provides no significant information about their presence in the region. The spectra show similar absorptions like n-D class #6 at bands 3, 4, 5 and 7, which may be due to the presence of certain unaltered silicate minerals associated with other poorly altered minerals in the region. The mean spectra of n-D class #9 (about 7.8338 km^2 distinguished in the image purple pixels) occurs in the region of dyke and gabbro rocks and the derived materials are found in the wadi alluvium. This may be due to the presence of certain altered aluminosilicate minerals (Figure 8d) in the rocks. The n-D class #10 (about 0.0297 km^2 in coral color) shows poor occurrence of minerals and the spectra show absorption in band 4. This absorption may be due to the presence of silica in the poorly or unaltered silicate minerals.

MINERSLS MAPPING USING REMOTE SENSING DATA

Overall, it is interesting to observe that the SAM image is able to establish the occurrence and distribution of the major minerals of the region, which can be grouped into carbonate and silicate minerals. The occurrence of limestone rocks is clearly detected by the carbonate minerals. In addition, the occurrence of dyke and gabbros and derived materials found in the study region may be extrapolated from the distribution of silicate minerals. Therefore, in this study, the multispectral ASTER satellite data and applied image processing methods used provided information on the occurrence and spatial distribution of minerals of the limestone formations and associated rock types of the study region. Although the information is obtained from mixed pixels, a study using hyperspectral data with high spatial resolution could provide more details on the occurrence of minerals in the region.

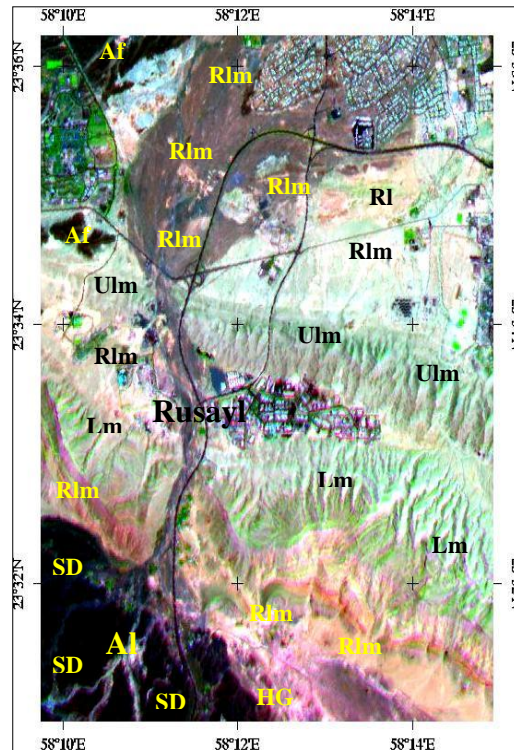


Figure 4. ASTER RGB color composite image (R:8; G:3; B:1) showing the rock types of the Rusayl and Al Jafnayn region (Rlm - Recent to Sub-Recent alluvial fans and wadi alluvium; Af - Ancient alluvial fans, terraces; RI - Reef limestone; Ulm - Upper nodular limestone; Lm - Lower nodular limestone; HG – High level gabbro; SD - Sheeted dyke).

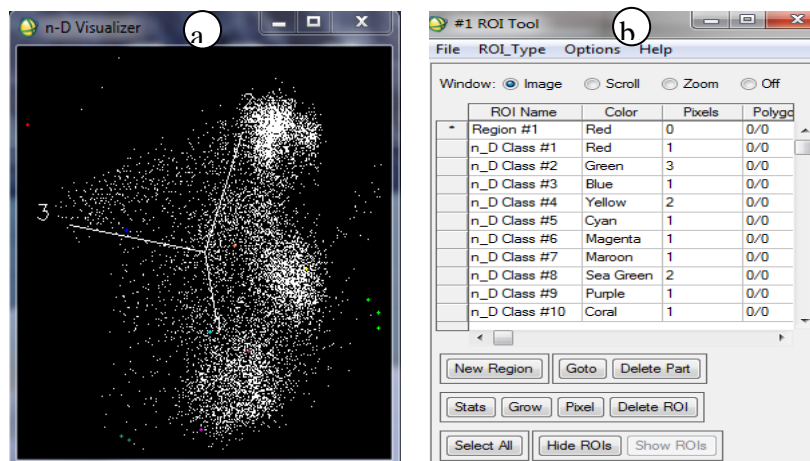


Figure 5. (a) n-Dimensional visualizer plot showing the group of pure pixels and endmembers, and (b) the number of pixels collected on the endmembers with the colors selected in n-Dimensional visualizer plot and for the discrimination.

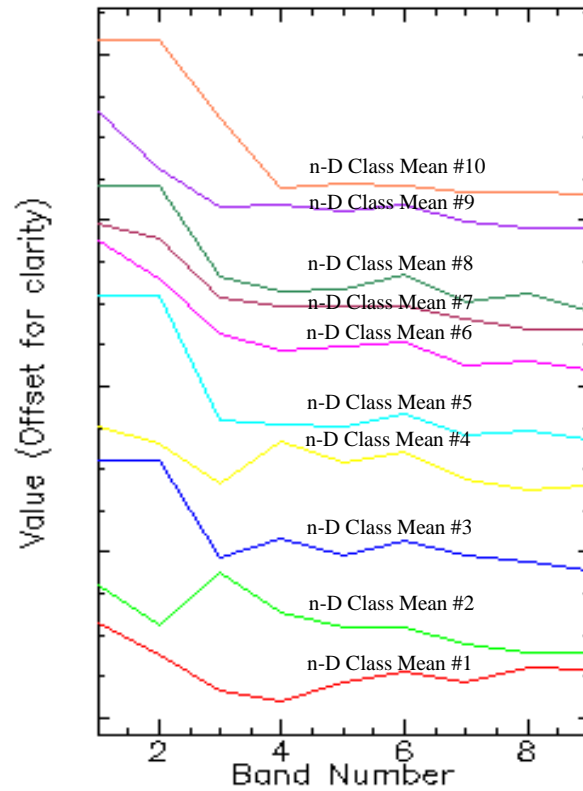


Figure 6. Plot of endmember spectra (Class Means) of Rusayl and Al Jafnayn region.

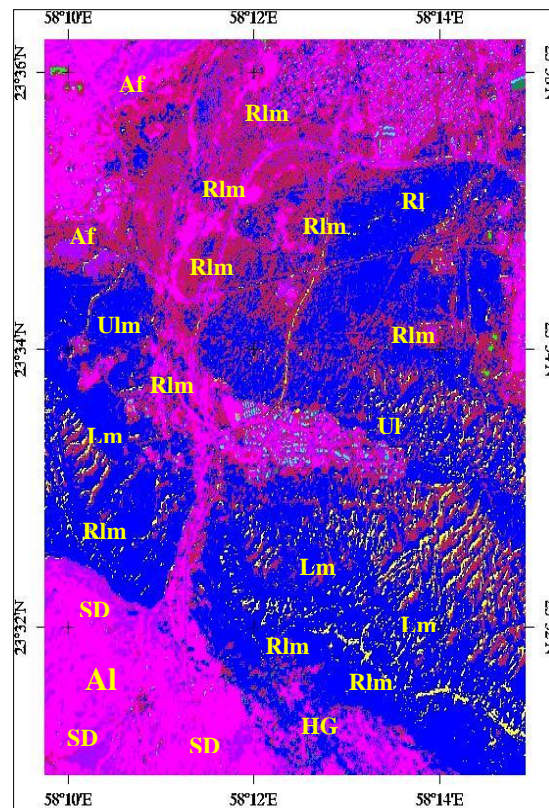


Figure 7. SAM classified image showing the mineral distribution in the Rusayl and Al Jafnayn region (Rlm - Recent to Sub-Recent alluvial fans and wadi alluvium; ; RI - Reef limestone; Af - Ancient alluvial fans, terraces; Ulm - Upper nodular limestone; Lm - Lower nodular limestone; HG – High level gabbro; SD - Sheeted dyke).

MINERSLS MAPPING USING REMOTE SENSING DATA

Table 2. Distribution of pixels in Rusayl and Al Jafnayn region in the SAM n-D classes.

n-D Classes ^a	No. of pixels	% in total area	Area in Km ²
n-D Class Mean #1	8052	2.508	1.8117
n-D Class Mean #2	199	0.062	0.0447
n-D Class Mean #3	134934	42.021	30.3601
n-D Class Mean #4	9248	2.88	2.0808
n-D Class Mean #5	1744	0.543	0.3924
n-D Class Mean #6	54468	16.962	12.2553
n-D Class Mean #7	76502	23.824	17.2129
n-D Class Mean #8	1018	0.317	0.229
n-D Class Mean #9	34817	10.843	7.8338
n-D Class Mean #10	132	0.041	0.0297
Total	321,114	100.001	72.2504

^a Unclassified: 0 points (0.000%) (0.0000 km²).

7. Field and Laboratory studies

Field work was conducted to confirm the image interpretation discussed and to validate the occurrence of the minerals and rocks of the study region. In the field, the lower and upper nodular limestone formations of Tertiary age are exposed well on the surface and crop out at Wadi Rusayl, near to Rusayl village in the study region. Along the wadi section, the formations exhibit nodular and massive limestones (Figure 9a and inset; S1 in Fig. 1b) with ophiolite clasts. The formations are conformable and occur above the yellow marl (Figure 9b; S2 in Figure 1b) and marly wackestone. The limestone formations are interbedded by multicoloured shale, sandstone and conglomerate (Figure 9c; S3 in Figure 1b), which can be observed in the road section. The lower part of the formation consists of bivalves, gastropods and small corals.

The upper boundary is conformable with the Rusayl Formation. The Rusayl Formation contains thick, resistant and nodular microcrystalline limestone followed by soft multicolored shale and marl. Exposures of shales and marls characterize the formation and are all highly weathered. The basal unit consists of poorly indurated, multicolored shale and marl with occasional thin and microcrystalline limestones. The presence of ancient alluvial fan and terrace deposit were verified in the field. The weathered surface materials occurring at ancient alluvial fans and terraces are a mixture of gabbro and mafic fragmented materials. These appear dark in color and are easily distinguishable (Figure 9d; S4 in Figure 1b). The surface materials on the terraces are loose, vary in size and are poor or unaltered (inset in Figure 9d). The deposits are cemented by lime materials observed along the road section (Figure 9e; S5 in Figure 1b). The recent wadi alluviums are friable, loose, vary in size and are poor or unaltered (Figure 9f; S6 in Figure 1b) on the surface below which the materials are cemented. The occurrence of calcrete in the wadi deposits can be observed. The study of samples under the microscope shows the frequent presence of major carbonate minerals and shells (Figure 9g, h) in the limestone formations.

The barren exposures of doleritic and basaltic sheeted dykes and high level gabbro occurring near to Al Jafnayn are verified in the road cuttings. The sheeted dykes vary in thickness, dark green to green in colour, fine grained and exhibit chilled margins (Figure 10a, b and inset; S7 in Figure 1b). Epidotization is observed in the dyke rocks (Figure 10c). The vertical foliated gabbro (Figure 10d; S8 in Figure 1b) shows alternate layering of light and dark colored felsic and mafic rich minerals (Figure 10e). Under the microscope, the dyke shows the presence of major minerals such as plagioclase feldspar, pyroxene and magnetite (Figure 10f, g). Very few grains of olivine were observed. The gabbro consists of mineral assemblages of olivine, hornblende, calcic-plagioclase and pyroxene (Figure 10h). Plagioclase occurs as subhedral grains.

During the study, spectral measurements were taken over the limestone formations at different locations in the field, and in the laboratory on the samples collected, using a portable PIMA SP infrared spectrometer to confirm the occurrence and spectral absorption characters of minerals. The selected spectra collected over the limestones are given in the spectral plot (Figure 11a, measurements around S2, S3 and S5 and lab samples). The collection of spectra in the SWIR region, with a spectral resolution of 7 nm over the rocks, show narrow absorption sharp features at nearly 1400 nm, 1900 nm, and 2300 nm, and are well comparable with the studied spectra (Figure 3). The absorptions are mainly due to the presence of major carbonate minerals, namely dolomite (Ca Mg (CO₃)₂), and hydroxyl group bearing clay mineral, namely montmorillonite in the samples. The spectra of gabbros (Figure 11b, measurements around S8 and near S7 and lab samples) show absorptions around 2250 nm and 2350 nm. The absorption near 2250 nm may be due to the influence of clinopyroxene minerals, and the absorptions near 2350 nm are due to the presence of OH bearing epidote and chlorite minerals in the rock.

The study of spectra in the range of 300–3000 nm wavelength over the dyke rocks may provide more information on the occurrence of silicate minerals. The presence of abundant minerals of dolomite in limestones and of epidote, hornblende and chlorite minerals in gabbro rock samples were confirmed by XRD analyses (Figures 11c, d).

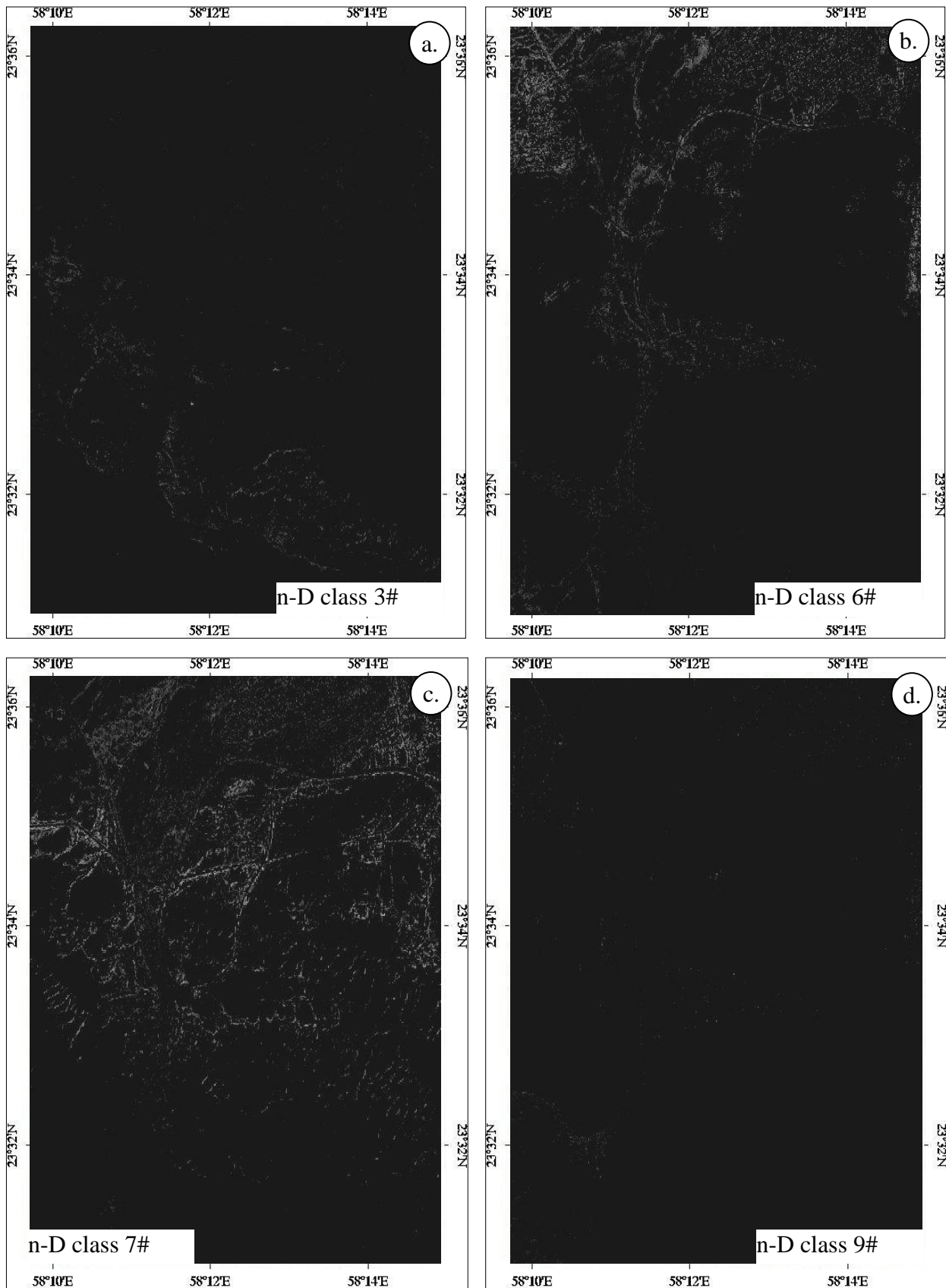


Figure 8. The images of n-D classes showing the distribution of (a) dolomites, (b) and (c) silicates and (d) altered aluminium silicate minerals of the Rusayl and Al Jafnayn region.

MINERSLS MAPPING USING REMOTE SENSING DATA

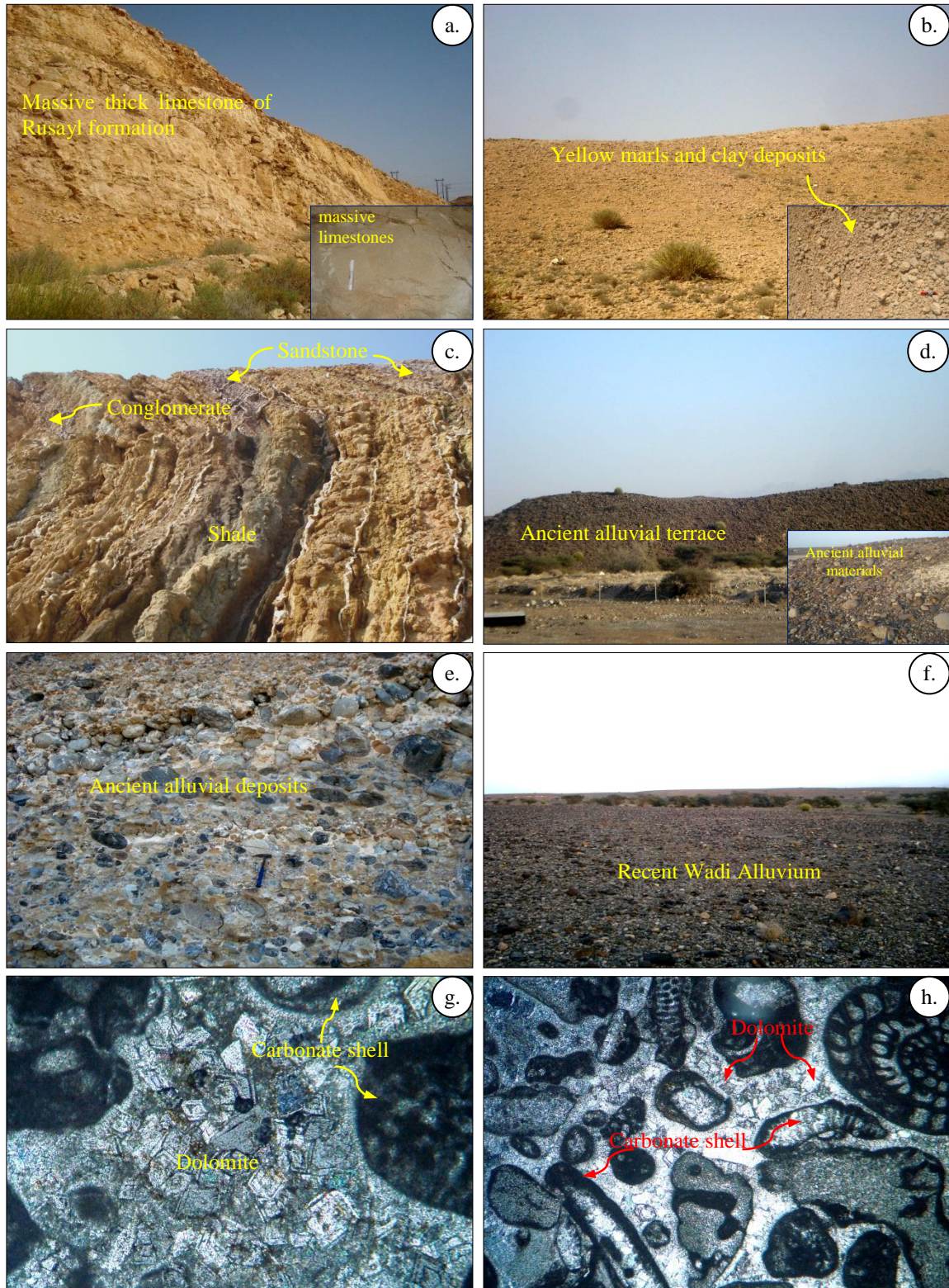


Figure 9. Field photographs showing (a) the massive Rusayl limestone formation (S1 in Figure 1b), (b) the occurrence of friable yellow marls and clays (S2 in Figure 1b), (c) the occurrences of interbedded multicoloured shale, sandstone and conglomerate (S3 in Figure 1b), (d) the ancient alluvial terrace materials (S4 in Figure 1b), (e) the ophiolite clasts in the limestone cements (S5 in Figure 1b), (f) the recent alluvial materials (S6 in Figure 1b), and the microphotographs show (g) the dolomite minerals of massive limestones and (h) the fossil limestones (nicols crossed, 25x).

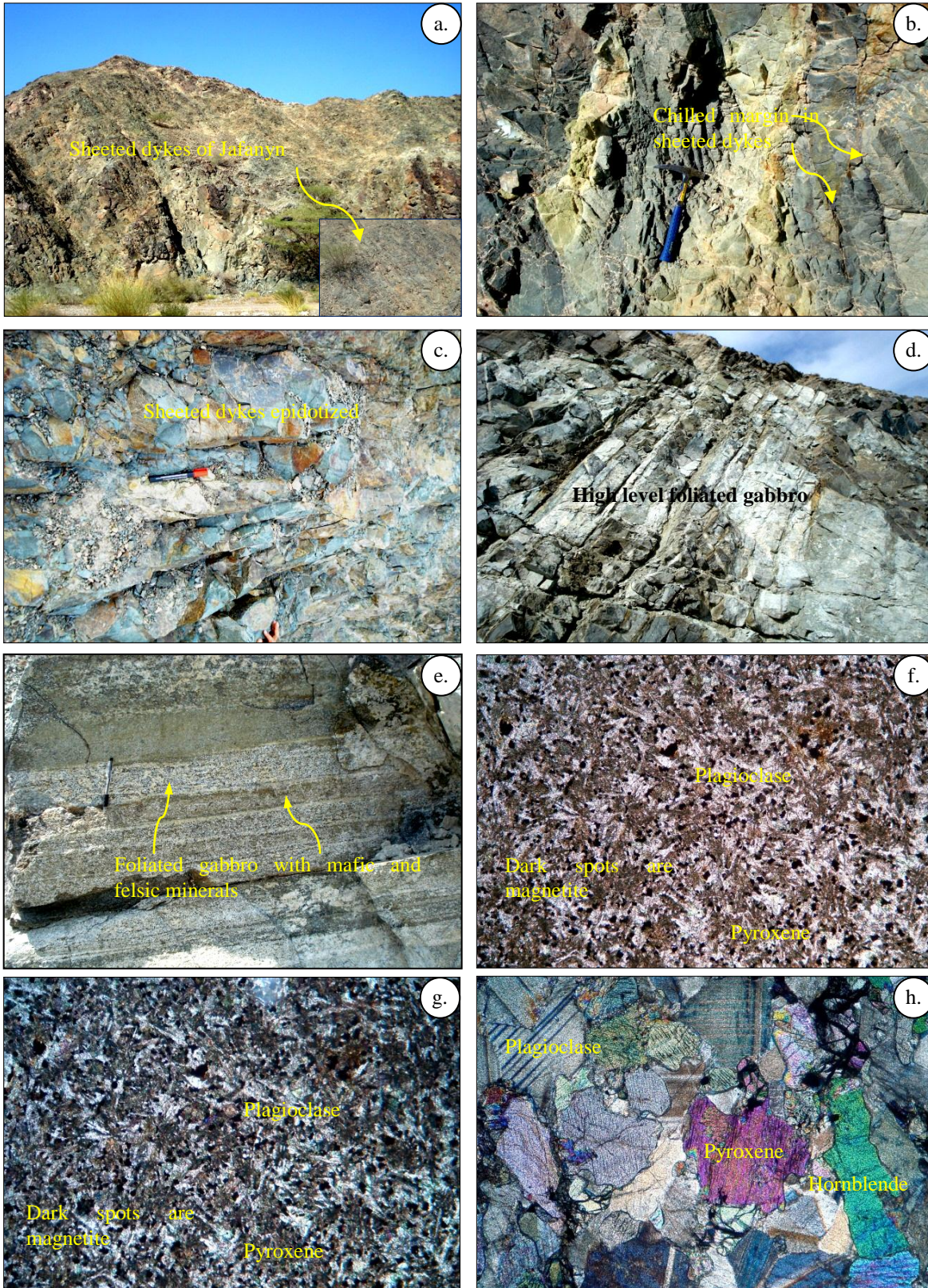


Figure 10. Field photographs show the occurrence of (a) and (b) the sheeted dykes (S7 in Figure 1b), (c) the chilled margin of the dykes (S7 in Figure 1b), (d) the high level foliated gabbros (S8 in Figure 1b), (e) the foliated gabbro shows the presence of mafic and felsic minerals (S8 in Figure 1b), and the microphotographs show the minerals of sheeted dykes (f) nicols parallel (35x) and (g) nicols crossed (35x) and (h) gabbro (nicols crossed, 25x).

MINERSLS MAPPING USING REMOTE SENSING DATA

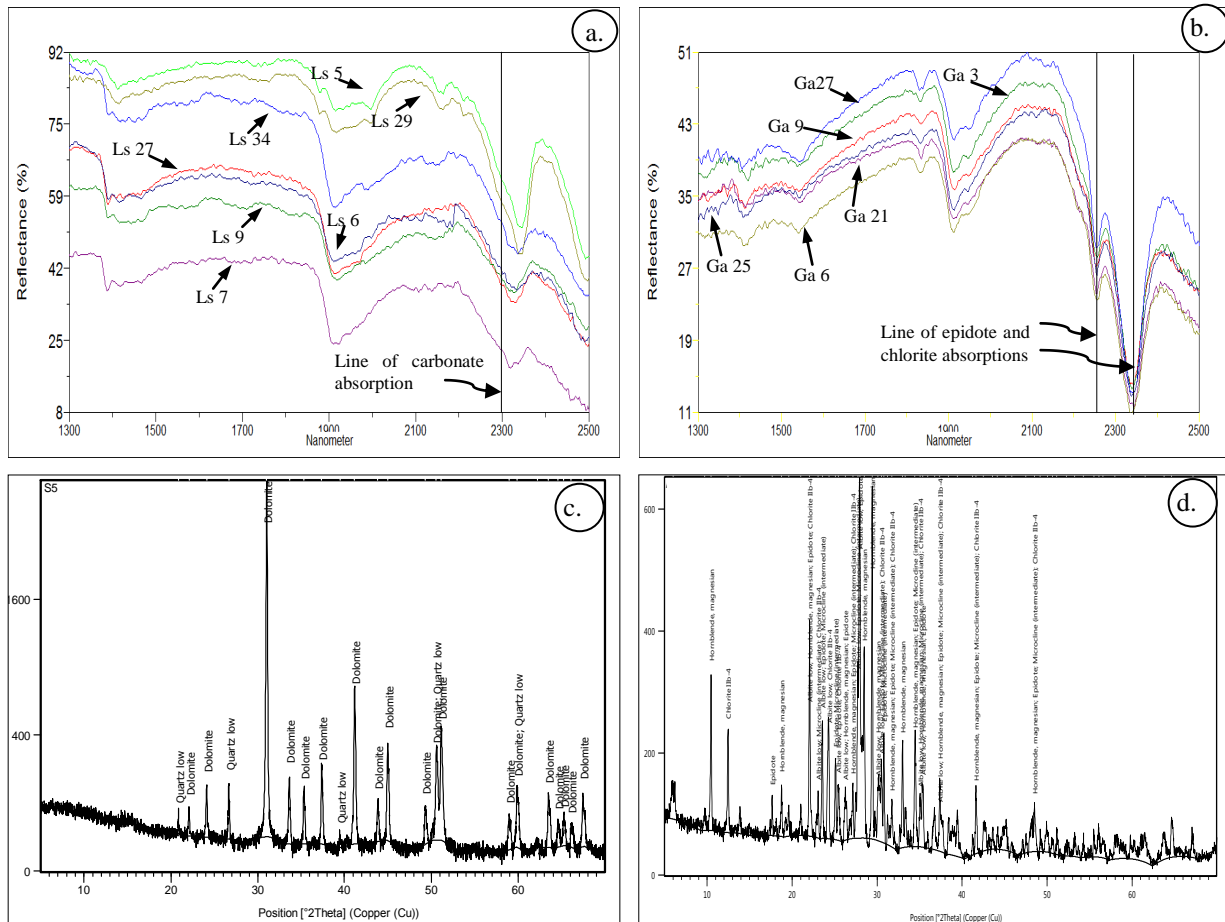


Figure 11. Laboratory spectral plots showing (a) carbonates absorptions in limestones, (b) epidote and chlorite OH absorptions in gabbros. The results of XRD of the limestones show the presence of abundance of dolomite minerals and the gabbros show the occurrence of epidote, hornblende and chlorite minerals in Rusayl and Al Jafnayn region.

8. Conclusion

In the present study, the occurrence of minerals in the rocks of the Rusayl and Al Jafnayn regions, Muscat, the Sultanate of Oman is studied using the ASTER VNIR-SWR spectral bands, and by the SAM supervised classification image processing method. The results of SAM clearly show the occurrence of carbonate minerals in limestone bearing rocks and silicate minerals in the dyke rocks, and their spatial distributions. The image interpretations are verified in the field by identification of minerals and rocks, and confirmed through laboratory analyses. The study has proved that the technique is time and cost-effective in comparison to the time consuming classical field mapping of minerals and rocks, and can be used in the difficult terrain of other similarly arid regions not reachable for conventional geological mapping and where it is difficult to do exhaustive sampling.

9. Acknowledgements

The authors are thankful to NASA Land Processes Distributed Active Archive Center User Services, USGS Earth Resources Observation and Science (EROS) Center (<https://LPDAAC.usgs.gov>) for providing the ASTER data. The study is supported by Sultan Qaboos University Internal Grant IG/SCI/ETHS/14/02. XRD analytical help was extended by Mr. Saif Amer Al-Maamari, CAARU. The authors are thankful to the anonymous reviewers and to the editor of the journal for their valuable reviews and for providing comments and suggestions that have helped to improve the manuscript.

References

1. Abrams, M.J., Rothery, D.A. and Pontual, A. Mapping in the Oman ophiolite using enhanced landsat thematic mapper images. *Tectonophys.*, 1988, **151**, 387-401.
2. Bedell, R.L. Geological mapping with ASTER satellite: new global satellite data that is a significant leap in remote sensing geologic and alteration mapping. *Special Publication Geol. Soc. Nevada*, 2001, **33**, 329-334.
3. Ramadan, T. and Kontny, A. Mineralogical and structural characterization of alteration zones detected by orbital remote sensing at Shalatein District, SE Desert, Egypt. *J. Afr. Earth Sci.*, 2004, **40**, 89-99.
4. Gad, S. and Kusky, T.M. Lithological mapping in the eastern desert of Egypt, the Barramiya area, using landsat thematic mapper (TM). *J. Afr. Earth Sci.*, 2006, **44**, 196-202.
5. Zhang, X., Pazner, M., Duke, N. Lithologic and mineral information extraction for gold exploration using ASTER data in the south Chocolate Mountains (California). *Photogrammetry & Remote Sensing*, 2007, **62**, 271-282.
6. Amer, R., Kusky, T.M. and Ghulam, A. Lithological mapping in the central eastern desert of Egypt using ASTER data. *J. Afr. Earth Sci.*, 2010, **56(2-3)**, 75-82.
7. Rajendran, S., Thirunavukkarasu. A. Balamurugan. G. and Shankar. K. Discrimination of iron ore deposits of granulite terrain of Southern Peninsular India using ASTER data. *J. Asian Earth Sci.*, 2011a, **41**, 99-106.
8. Tangestani, M.H., Jaffari, L. Vincent, R.K. and Maruthi, S.B.B. Spectral characterization and ASTER-based lithological mapping of an ophiolite complex: A case study from Neyriz ophiolite, SW Iran. *Remote Sensing Environ.*, 2011, **115**, 2243-2254.
9. Rajendran, S. and Nasir, S. Aster spectral analysis of ultramafic lamprophyres (carbonatites and aillikites) within the Batain nappe, northeastern margin of Oman - a proposal developed for spectral absorption. *Int. J. Remote Sensing*, 2013, **34(8)**, 2763-2795.
10. Rajendran, S., Hersi, Al-Harthy, O.S., Al-Wardi, A.R., El-Ghali, A.M. and Al-Abri A.H. Capability of Advanced Spaceborne Thermal Emission and Reflection Radiometer (ASTER) on discrimination of carbonates and associated rocks and mineral identification of eastern mountain region (Saih Hatat Window) of Sultanate of Oman. *Carbonates and Evaporites*, 2011b, **26**, 351-364.
11. Rajendran, S., Al-Khirbash, S., Nasir, S., Al-Abri, A.H., Kusky, T.M. and Ghulam, A. ASTER detection of chromite bearing mineralized zones in Semail Ophiolite Massifs of the northern Oman mountain: exploration strategy. *Ore Geol. Rev.*, 2012, **44**, 121-135.
12. Rajendran, S., Nasir, S., Kusky, T.M., Ghulam, A., Gabr, S. and El-Ghali, M. Detection of hydrothermal mineralized zones associated with Listwaenites rocks in the Central Oman using ASTER data. *Ore Geo. Rev.*, 2013, **53**, 470-488.
13. Pinet, P., Harris, E., Python, M., Ceuleneer, G., Launeau, P., Daydou, Y., Cord, A., Al Azri, H., Chabrilat, S., Lenot, X. and Chevrel, S. Hyperspectral Remote Sensing Approach for Rock Surface Mineralogy Mapping in Arid Environment. IUGG XXXIII General Assembly, International Union of Geodesy and Geophys. Sapporo, Japan, 2003.
14. Pinet, P.C., Clenet, H., Rosemberg, C., Ceuleneer, G., Heuripeau, F., Harris, E., Daydou, Y., Baratoux, D., Chevrel, S., Launeau, P., Combes, J-P., Lemouelic, S. and Sotin, C. *Mantle Rock Surface Mineralogy Mapping in Arid Environment from Imaging Spectroscopy: The Case of the Maqsad Peridotitic Massif in Oman and Implications for the Spectroscopic Study of Exposed Mafic Units on Mars*, LPSC 37th, Houston, # 1346, 2006.
15. Combe, J.P., Launeau, P. Pinet, P. Despan, D. Harris, E. Ceuleneer, G. and Sotin, C. Mapping of an ophiolite complex by high-resolution visible-infrared spectrometry. *Geochem. Geophys. Geosystems*, 2006, **7(8)**, 1-11.
16. Clenet, H., Pinet, Daydou, P.C. Heuripeau, Y. Rosemberg, F. and C. Ceuleneer, G. A sytematic testing approach using the Modified Gaussian Model (MGM) for mafic mineralogy mapping in natural conditions (Earth, Mars). *Proc. Lunar Planetary Sci. Conf. XXXIX*. 2008.
17. Roy, R., Launeau, P. Carrere, V. Pinet, P.C. Ceuleneer, G. Clenet, H. Daydou, Y. Girardeau, J. and Amri, I. Geological mapping strategy using VNIR hyperspectral remote sensing: application to the Oman ophiolite (Sumail Massif). *Geochem. Geophys. Geosystems*, 10: Q02004. doi:10.1029/2008GC002154, 2008.
18. Clenet, H., Ceuleneer, G., Pinet, P., Abily, B., Daydou, Y., Harris, E., Amri, I. and Dantas, C. Thick sections of layered ultramafic cumulates in the Oman ophiolite revealed by an airborne hyperspectral survey: petrogenesis and relationship to mantle diapirism. *Lithos.*, 2010, **114**, 265-281.
19. Rajendran, S. and Nasir, S. ASTER spectral sensitivity of carbonate rocks - study in sultanate of Oman, *Adv. Space Res.*, 2014b, **53**, 656-673.
20. Robertson A.H.F. and Searle, M.P. The Northern Oman Tethyan Continental Margin: stratigraphy, structure, concepts and controversies, the geology and tectonics of the Oman region. *The Geol. Soc., London*, 1990, **49**, 3-25.
21. Ministry of Petroleum and Minerals, *Geological Map, Oman* (1:100,000). SEEB Sheet NF 40-3C, 1986.
22. Gupta, R.P. *Remote Sensing Geology*. 2nd Ed., Springer, Heidelberg, 2003.
23. Clark, R.N., King, T.V.V. Klejwa, M. Swayze, G.A. and Vergo, N. High spectral resolution reflectance spectroscopy of minerals. *J. Geophys. Res.*, 1990, **95**, 12653-12680.
24. Van der MEER, F. Spectral reflectance of carbonate mineral mixtures and bidirectional reflectance theory: quantitative analysis techniques for application in remote sensing. *Remote Sensing Rev.*, 1995, **13**, 67-94.

MINERSLS MAPPING USING REMOTE SENSING DATA

25. Clark, R.N. and Roush, T.L. Reflectance spectroscopy: quantitative analysis techniques for remote sensing applications. *J. Geophys. Res.*, 1984, **89**, 6329-6340.
26. Gaffey, S.J. Reflectance spectroscopy in the visible and near infrared (0.35-2.55 microns): applications in carbonate petrology. *Geol.*, 1985, **13**, 270-273.
27. Gaffey, S.J. Spectral reflectance of carbonate minerals in the visible and near infrared (0.35-2.55 microns): calcite, aragonite, and dolomite. *Am. Miner.*, 1986, **71**, 151-162
28. Gaffey, S.J. Spectral reflectance of carbonate minerals in the visible and near infrared (0.35-2.55 microns): anhydrous carbonate minerals. *J. Geophys. Res.*, 1987, **92(B2)**, 1429-1440.
29. Crowley, J.K. Visible and near-infrared spectra of carbonate rocks: Reflectance variations related to petrographic texture and impurities. *J. Geophys. Res.*, 1986, **91(B5)**, 5001-5012.
30. Hunt, G.R. Spectroscopic Properties of Rocks and Minerals. In: Carmichael, R.S. (Ed.), *Handbook of Physical Properties of Rock*. CRC Press, Boca Raton, 1982, **1**, 295-385.
31. Hunt, G.R. Spectral signatures of particulate minerals in the visible and near infrared. *Geophys.* 1977, **42**, 501-513.
32. Hunt, G.R. and Salisbury, J.W. Visible and near infrared spectra of minerals and rocks: II. Carbonates. *Mod. Geol.*, 1971, **2**, 23-30.
33. Hunt, G.R. and Salisbury, J.W. Visible and near infrared spectra of minerals and rocks: I. Silicate minerals. *Mod. Geol.*, 1970, **1**, 283-300.
34. Hunt, G.R., Salisbury, J.W. and Lenhoff, C.J. Visible and near-infrared spectra of minerals and rocks. IX, Basic and ultrabasic igneous rocks, *Mod. Geol.*, 1974, **5**, 15-22.
35. Hunt, G.R. and Ashley, P. Spectra of altered rocks in the visible and near infrared. *Eco. Geol.* 1979, **74**, 1613-1629.
36. Blom, R.G., Abrams, M.J. and Adams, H.G. Spectral reflectance and discrimination of plutonic rocks in the 0.45 to 2.45 μm region. *J. Geophys. Res.*, 1980, **85**, 2638-2648.
37. Hunt, G.R. Near-infrared (1.3-2.4) spectra of alteration minerals-potential for use in remote sensing. *Geophys.*, 1979, **44(12)**, 1974-1986.
38. Clark, R.N. *Spectroscopy of Rock and Minerals and Principles of Spectroscopy*. In: Rencz, A.N. (Ed.), *Remote Sensing for the Earth Sciences: Manual of Remote Sensing*. 3th Ed., Vol.3, John Wiley & Sons, New York, 1999, 3-58.
39. Rajendran, S. and Nasir, S. ASTER mapping of limestone formations and study of caves, springs and depressions in parts of Sultanate of Oman, *Environ. Earth Sci.*, 2014a, **71**, 133-146.
40. Mars J.C. and Rowan L.C. Spectral assessment of new ASTER SWIR surface reflectance data products for spectroscopic mapping of rocks and minerals. *Remote Sensing Environ.*, 2010, **114**, 2011-2025.
41. Gad, S. Kusky, T.M. ASTER spectral ratioing for lithological mapping in the Arabian-Nubian shield, the Neoproterozoic Wadi Kid area, Sinai, Egypt. *Gondwana Res.*, 2007, **11(3)**, 326-335.
42. Rowan, L.C. and Mars, J.C. Lithologic mapping in the Mountain Pass Area, California using advanced spaceborne thermal emission and reflection radiometer (ASTER) Data. *Remote Sensing Environ.*, 2003, **84**, 350-66.
43. Ninomiya, Y. Mapping quartz, carbonate minerals and mafic-ultramafic rocks using remotely sensed multispectral thermal infrared ASTER data. *SPIE*, 2002, **4710**, 191-202.
44. Abdeen, M.M., Thurmond, A.K. Abdelsalam, M.G. and Stern, R.J. Use of TERRA ASTER band-ratio images for geological mapping in arid regions: the Neoproterozoic Allaqi suture, Egypt. *J. Remote. Sens. & Space Sci.*, 2002, **5**, 19-40.
45. Galvao, L.S., Filho, R.A. and Vitorello, C. Spectral discrimination of hydrothermal altered materials using ASTER Short-wave infrared bands, evaluation in a tropical Savannah Environment. *Inter. J. Appl. Earth Obs. Geoinfor.*, 2005, **7**, 107-114.
46. Mars, J.C. and Rowan, L.C. Regional mapping of phyllic- and argillic-altered rocks in the Zagros magmatic arc, Iran, using Advanced Spaceborne Thermal Emission and Reflection Radiometer (ASTER) data and logical operator algorithms. *Geosphere*, 2006, **2(3)**, 161-186.
47. Abrams, M. and Hook, S.J. Simulated ASTER data for geologic studies. *IEEE Trans. Geosci. Remote Sens.*, 1995, **33(3)**.
48. Rajendran, S., Nasir, S. Kusky T.M. and Al-Khribash, S. Remote sensing based approach for mapping of CO₂ sequestered regions in Semail Ophiolite Massifs of the Sultanate of Oman. *Earth Sci. Rev.*, 2014, **135**, 122-140.
49. Kruse, F.A., Boardman, J.W. and Hunnington, J.F. Comparison of airborne hyperspectral data and EO-1 Hyperion for mineral mapping. *IEEE Trans. Geosci. Remote Sensing*, 2003, **41(6)**, 1388-1400.
50. Gabr, S., Ghulam, A. and Kusky, T. Detecting areas of high-potential gold mineralization using ASTER data. *Ore Deposit Rev.*, 2010, **38**, 59-69. 2010.
51. Rajendran, S and Nasir, S. 2014c. Hydrothermal altered serpentinitized zone and a study of Ni-magnesioferrite-magnetite-awaruite occurrences in Wadi Hibi, Northern Oman Mountain: discrimination through ASTER mapping, *Ore Geol. Rev.*, **62**, 211-226.
52. Hecker, C.A., van der Meijde, M., van der Werff, H.M.A. and van der Meer, F.D. Assessing the influence of reference spectra on synthetic SAM classification results. *IEEE Trans. Geosci. and Remote Sensing*, 2008, **46(12)**, 4162-4172.

53. Kruse, F.A., Lefkoff, A.B. Boardman, J.B. Heidebreicht, K.B. Shapiro, A.T. and Barloon, P.J. The spectral image processing system (SIPS)-interactive visualization and analysis of imaging spectrometer data. *Remote Sensing Environ.*, 1993, **44**: 145-163.
 54. Boardman, J.W. and Kruse, F.A. Automated spectral analysis: a geological example using AVIRIS data, north Grapevine Mountains, Nevada. *Proc., ERIM Tenth Thematic Conference on Geologic Remote Sensing. Environmental Research Institute of Michigan*, Ann Arbor, MI, 1994, I-407-I-418.
-

Received 2 March 2014

Accepted 15 June 2014